AIAA JOURNAL
Vol. 34, No. 3, March 1996

Long-Range Schmidt–Cassegrain Laser Velocimeter for Large Wind-Tunnel Applications

Stephen E. Dunagan*
NASA Ames Research Center, Moffett Field, California 94035-1000

A two-component dual-beam laser velocimeter was designed and fabricated for use in the NASA Ames 40 × 80 ft wind tunnel. The instrument design was predicated on the use of inexpensive, high-quality, large-aperture Schmidt–Cassegrain telescope optics to perform both the laser beam focusing and scattered light collection functions. The instrument was configured to measure the streamwise and cross-stream components of velocity and enclosed in a streamlined optical assembly mounted on a two-dimensional traverse on the floor of the test section. The laser velocimeter probe volume was translated in the vertical direction by means of zoom optics. Coaxial backscattered light was collected through the same optical system and analyzed for Doppler shift. Single-mode polarization-maintaining fiber optics transmitted light from the remotely located laser into the optical assembly. A multimode fiber conveyed the scattered light to remotely located photodetectors. Standard frequency domain processing permitted analysis of Doppler signals with very poor signal-to-noise ratio. The system was evaluated in an optics laboratory in preparation for wind-tunnel test program applications. Sample data from this evaluation were presented as representative of the capability of the instrument.

Statement of the Problem

In recent decades the laser Doppler velocimeter[1] (LV) has seen increasing application to the study of aerodynamic phenomena. The LV provides a noninvasive measurement capability that is critical for the study of many phenomena. The dual-beam or differential-Doppler configuration of the instrument[2] has been shown to have many practical advantages and is used extensively in small-scale wind-tunnel testing. Although several new techniques offer increased potential for global measurement capability,[3,4] the LV remains a very important instrument for any aeronautical research facility.

Although significant progress has been made,[5] LV has not been widely used in large-scale wind-tunnel testing. To maintain the noninvasive quality of the measurement, it is necessary to place the instrument outside the wind-tunnel test section, or at least far enough away to limit its effect on the flowfield of interest. In large-scale wind tunnels, this means large separation between the probe volume (laser beam intersection volume) where Doppler shifted light is scattered and the receiving optics where that light is collected and focused on a photodetector. This large separation or long-range operation requirement demands high laser power density in the probe volume to achieve high scattered intensity of the Doppler shifted light and a large collection solid angle to concentrate it on the photodetector.

For a closed jet wind tunnel, it is further necessary to use windows of sufficient quality that the laser beams launched into the test section as well as the scattered light collected from the probe volume are not significantly degraded. In particular, the laser beams must not be refracted by striae in the windows so as to significantly reduce beam overlap in the probe volume. The window aperture must be sufficient to access the entire flow region of interest.

The National Full-Scale Aerodynamics Complex at NASA Ames Research Center is composed of two large wind tunnels and a static (hover) test facility. The 40 × 80 ft wind tunnel is the smaller of the two wind tunnels, with a speed capability up to 300 kn (154 m/s). It is a closed-loop tunnel with a closed, oval test section 80 ft in length. This tunnel is used extensively for performance, stability, and aeroacoustic testing. The instrument described in this paper is designed specifically for this facility.

The test section incorporates door and fragmentation shield structures that significantly limit optical access to the test section from the outside. This limitation, in conjunction with the very high cost of large-aperture high-quality optical windows, suggests an approach where the LV is mounted inside the test section.

The LV will be needed for a variety of test applications and must provide access to most of the test section volume. This is best accomplished with minimal flow intrusion if a two-component traverse is attached to the floor of the wind tunnel and the third traverse component is obtained by optically zooming the probe volume vertically, as seen in Fig. 1. This configuration is capable of measuring the streamwise and cross-stream velocity components at the same time from the single optical assembly. A second optical assembly or enhanced mode light detection and ranging (LIDAR) design[6] could be used to measure the vertical velocity component.

Facility characteristics dictate the specification of several system parameters.

1) The optical system must operate in confocal backscatter collection mode to accommodate zoom translation of the probe volume. This will adversely affect signal-to-noise ratio as well as the ability to make measurements close to horizontal model surfaces.

2) The vertical zoom range of the instrument will be from 3 to 8 m, with a design optimum at 5 m. This range will access 65% of the vertical dimension of the test section.

3) Long-range operation requires that the largest practical collector aperture be used. An aperture of 0.5 m would be required to match the collection solid angle of small-scale instruments.

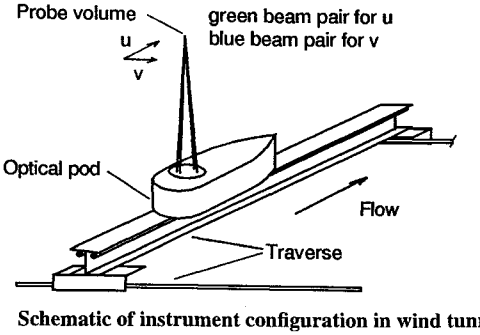

Fig. 1 Schematic of instrument configuration in wind tunnel.

Presented as Paper 95-0019 at the AIAA 33rd Aerospace Sciences Meeting, Reno, NV, Jan. 9–12, 1995; received Jan. 23, 1995; revision received July 31, 1995; accepted for publication Aug. 8, 1995.

*Aerospace Engineer, Rotorcraft Aeromechanics Branch.

4) The intrusive part of the LV must be small and streamlined but provide the required aperture.

These requirements are the basis for instrument design. This paper describes an approach that relies on the use of commercially available large-aperture astronomical telescope optics and the modification of these systems to perform the optical functions associated with LV.

Instrument Description

Design Considerations

Several design objectives may be identified. First, all design features must concentrate on enhancing signal power. A second related objective must be to reduce noise sources. Third, the system must be compact. These overarching objectives must be integrated with the more concrete requirements for sensitivity, spatial resolution, accuracy, and precision in the context of expected applications.

To increase signal power it is important to maximize the energy density within the probe volume. This may be accomplished by using the most laser power available or by focusing the probe volume to the minimum possible diameter, or both. Laser power is limited by cost or by fiber-optic transmission capabilities, which will be discussed more later. The lower limit for probe volume diameter is determined by signal processing considerations. In general, it is desirable to make the ratio of probe volume diameter D to fringe spacing d as large as possible. This provides many fringes in the probe volume and therefore many cycles for a signal processor to analyze. This is important for both counter and autocorrelation signal processing.

Confocal backscatter collection is inherently noisy. Since the same optical system is used to focus the laser beams to the probe volume and collect the scattered Doppler-shifted light, scattering from contaminants on the surface of the optics is a strong noise source. Furthermore, the close proximity of the laser beams and the light collection path permits scattered light from particles outside the probe volume to reach the photodetector. The surface glare that occurs where the laser beams that have passed through the probe volume strike the (possibly near) model surface or the distant wall of the wind tunnel is also near the signal light collection path. Spatial filtering is the most effective mechanism for reducing these noise sources. A spatial filtering pinhole works most effectively when the probe volume is small and the imaging capability of the collector is good.

The requirement for a compact probe assembly suggests a design with miniaturized components. The target of 0.5 m for the collector aperture presents a lower limit to the size of the optical assembly. Although miniature diode lasers have improved greatly in recent years in both beam power and beam quality, they are still of considerably lower quality than gas lasers. Fiber optics have been used successfully in LV applications for the transmission of laser light to the probe volume, as well as the transmission of collected light to the photodetector, and permit the laser to be removed from the probe assembly to some remote location outside the test section. However, the polarization-maintaining single-mode fibers required to maintain coherence and polarization in the laser beams must be of very small diameter and consequently can only transmit on the order of a few watts per fiber. Although this power limitation continues to improve with improving fiber and beam-coupling technology, the use of fiber optics for laser beam transmission limits the use of maximum laser power.

A balance of these somewhat conflicting objectives has been pursued with this design. The use of single-mode fibers will limit laser power to a few watts per fiber. The probe volume diameter will be minimized to increase the power density in the probe volume and thus maximize the scattered light intensity for individual particles. The ratio of probe volume diameter to fringe spacing will be maintained near 10 to provide adequate cycles in the Doppler burst for signal processing.

Telescope Optics

In recent years, advanced manufacturing techniques (for the aspheric corrector lens) have made a variety of low-cost Schmidt–Cassegrain telescopes commercially available, with apertures up to 400 mm. Although these units are designed for wide field imaging performance at infinite conjugate ratio, a methodology has been developed[7] to adapt them for on-axis imaging at conjugate ratios near unity. The optics may be configured either as a point focus collector, for use with off-axis designs, or as a confocal backscatter system that will focus the laser beams to form the probe volume and also collect the backscattered light. An example of a telescope modified for confocal backscatter operation is shown in Fig. 2. The corrector lens, primary mirror, and secondary mirror comprise the stock telescope. Modification typically requires replacement of the secondary mirror and/or repositioning of the three optical elements.

The modified Schmidt–Cassegrain system has several attractive features:

1) The imaging performance of the system, if properly modified, is nearly diffraction limited. This permits very efficient spatial filtering of the collected light to improve signal-to-noise ratio (particularly for small probe volumes).

2) Large-aperture systems may be purchased at a fraction of the cost of custom designed refractive optics and adapted with low-cost modification.

3) Because the high-power elements in these systems are reflector, chromatic aberration is virtually nonexistent. This permits two-color operation with no loss of imaging (spatial filtering) capability.

4) The folded Cassegrain design provides a very compact optical package.

5) The focusing translation of the primary mirror is readily adapted for zoom operation.

There are also some drawbacks to the use of modified telescope optics:

1) The limiting aperture for low conjugate ratio operation shifts from the corrector lens to the primary mirror, which increases the spacing from the probe volume to the limiting aperture and reduces collection solid angle.

2) The central obstruction of the secondary mirror blocks the central portion of the scattering cone and can significantly reduce the collection solid angle. These two light reduction effects become particularly acute as the operating distance to aperture ratio becomes small (less than 10).

3) Reflective optics are much more sensitive to vibration than refractive optics and care must be taken in the mounting of reflective elements to minimize vibration.

The attractive features just summarized are particularly important for this application. Despite the drawbacks, the Schmidt–Cassegrain optical design was chosen for this instrument.

Optical System Analysis

The relatively simple analytical approach employed here relied on a ray tracing analysis to evaluate the on-axis imaging performance

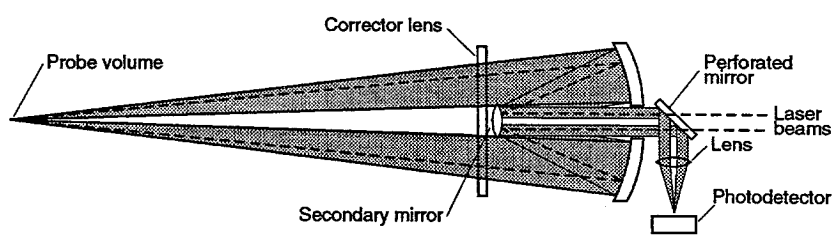

Fig. 2 Schmidt–Cassegrain telescope modified for confocal backscatter LV operation.

of the collector. The rms blur of ray bundles originating at the axis vertex in the object plane and converging to a best focus in the image plane was used as an indication of the imaging quality of the optical system. System magnification was evaluated from slight off-axis perturbations.

A paraxial Gaussian beam propagation calculation[8] was made to evaluate the expected beam waist locations and beam diameters at the various optical surfaces and at the probe volume. Collimating lenses for the single mode fiber output were selected based on this analysis to provide very small waist diameters at the probe volume. More details on these analyses may be found in Ref. 7.

Instrument Specifications

Based on the specified facility requirements and design philosophy, an instrument was designed, fabricated, and evaluated in large-scale testing. Figure 3 represents the optical layout of the instrument. A 6-W argon ion laser was used as the coherent source for the instrument. The blue (488 nm) and green (514 nm) lines were used to measure the streamwise and cross-stream components, respectively. The laser output is passed through two dispersion prisms to separate the 488- and 514-nm lines. Each beam was then passed through an acousto-optic cell adjusted to the Bragg angle. The amplitude of the driving waveform was adjusted to provide a 50:50 power ratio between the zero and first-order diffracted beams. The four resulting beams were then launched into four single-mode polarization-maintaining fibers using commercially available couplers.

The fibers conveyed the laser light to the optical probe assembly located inside the test section. The beams were recollimated by four lenses selected and adjusted to focus the beams to a waist located at the (probe volume) intersection of the beams. Transverse adjustment of these lenses also permitted the beams to be aligned parallel to the optical axis of the modified Schmidt–Cassegrain system. The secondary mirror expanded the beams to a large diameter at the primary mirror, which then focused them to a very small beam waist diameter at the beam intersection. The corrector lens served to correct beam astigmatism induced by off-axis propagation. Table 1 summarizes the prescription data for the Schmidt–Cassegrain optical system. Corrector lens and primary mirror data are for the stock telescope components. The secondary mirror data are for an

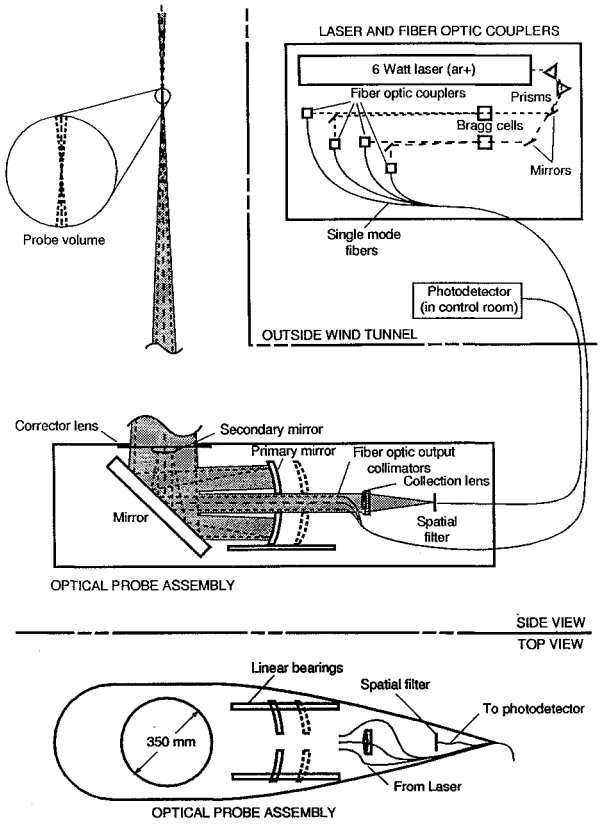

Fig. 3 Optical layout for Schmidt–Cassegrain laser velocimeter.

Table 1 General prescription data for the Schmidt–Cassegrain optical system

Parameter	Value
Aspheric corrector lens	
Diameter, m	0.356
Center thickness, m	0.00572
Refractive index	1.52
Corrector lens second-order aspheric constant A_2[a]	0.00380
Corrector lens fourth-order aspheric constant A_4[a]	−0.104
Primary mirror	
Diameter, m	0.362
Curvature, 1/m	0.656
Secondary mirror	
Spacing from front of corrector, m	0.063
Diameter, m	0.075
Curvature, 1/m	−3.213

[a]Surface contour of corrector lens front surface $z(r) = z_0 + A_2r^2 + A_4r^4$ (r is in meters).

appropriately chosen replacement, which was a lens with a high-reflection coating on the convex side.

As small particles pass through the probe volume, light is scattered in all directions, including back toward the optical system. This backscattered light is collected by the Schmidt–Cassegrain system and focused to a collimated wave, parallel to the incoming laser beams but traveling in the opposite direction. Some of the collimated backscattered light is blocked by the fiber mount and collimating lens apparatus, but these components were designed to minimize this blockage. A 300-mm focal length infinite conjugate ratio achromatic lens was used to focus the collimated light into a multimode fiber optic that transferred it to a photodetector located outside of the test section. A 50-μ spatial filtering pinhole was located in front of the fiber optic to reduce optical noise coming from light scattered from any point outside of the probe volume. This pinhole was sized to exactly match the probe volume diameter. Ray tracing analysis indicated that at 5-m range the pinhole rejected 90% of the light scattered from any of the beams, for any distance greater than 5 mm from the probe volume center. The output from the multimode fiber was collimated and passed through a dichroic beamsplitter to separate out the blue and green signal components. Optical interference filters were used to further block light at all but the correct wavelength. High-sensitivity, high-speed photomultiplier tubes converted the heterodyned Doppler-shifted light to an electrical signal.

Zoom Range Characteristics

The characteristics of the probe volume were different for the two laser wavelengths and continuously varied with operating range for this zoom design. These characteristics are summarized in Table 2 for the near focus, design, and far focus ranges (3, 5, and 8 m). The streamwise flow component u was measured by the 514-nm laser wavelength, whereas the cross-stream component v was measured by the 488-nm wavelength. It may be seen that the probe volume may be moved through its entire 5-m range by moving the primary mirror less than 12 cm. This permitted rapid scanning of the probe volume in the vertical direction. Both the probe volume diameter and the fringe spacing (governed by the beam convergence angle) increased with range. It is interesting to note that the number of fringes, which is the ratio of probe volume diameter to fringe spacing, remained constant for each wavelength. The magnification for the collection optics (i.e., ratio of object or probe volume diameter to image diameter at the spatial filter) decreased with range. But the optimum spatial filter size, which is the product of probe volume diameter and system magnification, remained constant for each wavelength. This was a very fortunate condition as it permitted effective spatial filtering through the entire zoom range without requiring a variable diameter spatial filter. The Rayleigh range (distance from beam waist to point of maximum wavefront curvature) at the probe volume also increased with range. The waist moved from inboard of the probe volume to outboard of the probe volume with increasing range. However, the probe volume to waist spacing was

Table 2 Probe volume and collection system characteristics

Parameter	Range 3m u	3m v	5m u	5m v	8m u	8m v
Design data (from ray trace and Gaussian beam propagation analysis)						
Laser wavelengths, μ	0.514	0.488	0.514	0.488	0.514	0.488
Primary mirror location,[a] m	0.855	0.855	0.783	0.783	0.740	0.740
Probe volume diameter, mm	0.063	0.058	0.103	0.095	0.163	0.150
Fringe spacing, μ	6.51	6.17	10.6	10.0	16.9	16.0
Number of fringes	9.70	9.42	9.69	9.42	9.68	9.41
Rayleigh range, mm	6.08	5.45	16.05	14.38	40.58	36.37
Beam waist to focus distance, mm	1.84	1.83	0.00	0.00	−5.26	−5.24
Collector system magnification	−0.464	−0.464	−0.286	−0.286	−0.180	−0.180
Optical spatial filter size, μ	29	27	29	27	29	27
Measured data						
Probe volume diameter, mm						
Zero-order beam	0.065	n/a	0.107	n/a	0.171	n/a
First-order beam	0.075	n/a	0.125	n/a	0.198	n/a

[a]From front surface of corrector lens.

Table 3 Probe volume parameter range curvefits

Parameter	Curvefit	c_1	c_2	c_3	R
Primary mirror loc.	$Z_p(r) = c_1 + c_2/(c_3 + r)$	0.84820	0.16065	0.05806	1.00000
Probe volume diameter	$d_0(r) = c_1 + c_2 r$	0.02257	0.97185	——	0.99999
Fringe spacing	$d_f(r) = c_1 + c_2 r$	0.02112	0.98194	——	0.99997
Inverse magnification	$1/M(r) = c_1 + c_2 r$	0.02898	0.97441	——	0.99998

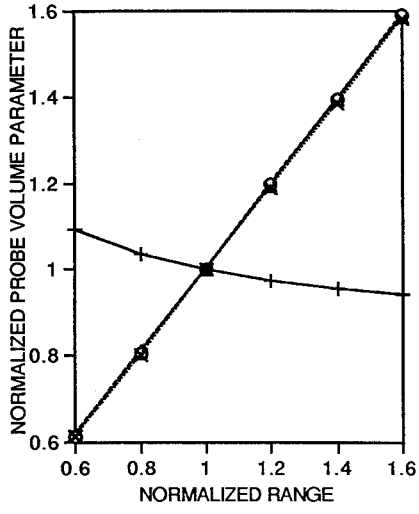

Fig. 4 Nondimensionalized probe volume parameters as a function of range: —┼—, primary position; —×—, probe volume diameter; - - -○- - -, fringe spacing; and —△—, inverse magnification.

never more than 33% of the Rayleigh range. This ensured minimal variations in fringe spacing (resulting from wavefront curvature) throughout the probe volume.

The prediction methodology for laser beam waist diameter and location calculations was based on Gaussian beam propagation theory. Beams propagating out from the single mode fibers were modeled as having a waist diameter equal to the mode field diameter located at the fiber surface. Real laser beams do not possess the ideal Gaussian profile shape. The degradation may be quantified in terms of the propagation constant M^2, which is simply the ratio of the actual beam waist diameter to the ideal Gaussian beam waist diameter and is always greater than 1. The beam waists for the green laser beams were measured with a spinning slit beam profiler and are presented in Table 2 for comparison with the predicted probe volume diameter. As would be expected, the measured waist diameters were found to be equal to or larger than the predicted Gaussian diameters. Furthermore, the propagation constant was not identical for beams emitted from different fibers. This condition was perhaps the result of irregularities in the fiber end faces.

Both the mirror spacing and fringe spacing as a function of range were needed for the calibration of the instrument. The functional form of the variation of these and other system parameters with range was examined empirically. Figure 4 shows primary mirror position Z_p, probe volume diameter d_0, fringe spacing d_f, and inverse magnification $1/M$ plotted as a function of range for the 514-nm wavelength. All parameters have been normalized by the design optimum (5-m range) values. The relationships for magnification, fringe spacing, and probe volume diameter are quite linear. The paraxial lens combination formula suggests a relationship between primary mirror position and probe volume range location as shown in Eq. (1):

$$Z_p(r) = c_1 + c_2/(c_3 + r) \tag{1}$$

where r is the range measured from the front surface of the corrector lens and c_1, c_2, and c_3 are determined by least-squares curvefitting. The curvefit data for these parameters for the 514-nm wavelength is given in Table 3. The correlation coefficient R is very good for all of the curvefits.

Translation Apparatus

As previously stated, the instrument achieved three-dimensional translation of the probe volume by translating the entire probe assembly in the cross-stream and streamwise directions and by optically zooming in the vertical direction. A two-component linear traverse mechanism capable of moving the system quickly and accurately over a large distance was needed. The design chosen for this instrument incorporated cylindrical case-hardened linear bearings and lead screws of the recirculating ball type. Stepping motors with digital controllers and optical encoder feedback were used to control the motion of the frame.

The initial test program for which this instrument was developed required only limited translation in the streamwise and cross-stream directions. A small prototype translation frame was built to provide a range of motion of plus or minus 0.6 m in the streamwise and 0.3 m in the cross-stream directions. The theoretical positioning resolution for linear translation was 0.025 mm, based on encoder resolution and lead screw pitch. Positioning resolution in the zoom direction was dependent on the linear encoder resolution and the derivative of the $Z_p(r)$ curve of Table 3. This computed resolution varied from 0.2 mm at 3-m range to 1.1 mm at 8-m range.

Signal Processing

The limited collection solid angle and confocal backscatter design for this system contributed to low signal-to-noise ratio on the Doppler signal. Although the spatial filtering mechanism was employed to improve this condition, the signal quality was not generally compatible with counter type signal processors that were used previously.[5] The limited number of fringes in the probe volume (10 or fewer) was another feature of this design that was problematic for counter processors.

Concurrent digital signal processing technology incorporated several approaches that greatly enhanced the ability to accurately extract the Doppler frequency from a noisy burst. Several processors based on the digital Fourier transform[9] (or some other closely related transform) or based on digital autocorrelation[10] were commercially available. Innovations that included quadrature down mixing, single bit digitization, frequency domain burst detection, and efficient transform algorithm structure permitted very rapid burst processing with data rates that rival and even exceed those of counter processors.

This system incorporated a commercial "real time signal analyzer"[11] having many of the features mentioned earlier. The processing bandwidth could be selected to provide as low as 12 m/s full-scale velocity at 3-m range to as high as 675 m/s full-scale velocity at 8-m range. The measurement resolution for the analyzer was 0.4% full scale.

Instrument Fabrication and Evaluation

Instrument components were purchased or fabricated and the instrument was assembled in an optics laboratory for initial checkout. Two types of single-mode polarization-maintaining fiber couplers were evaluated. A design providing six degrees-of-freedom adjustment was selected. These couplers were very difficult to align but provided minimum insertion loss and therefore permitted maximum laser power at the probe volume. The stainless steel construction of the couplers limited thermal drift. The system maintained alignment without significant loss of beam power coupled into the fibers for at least 8 h and for temperature fluctuations on the order of 10°C.

Efficient coupling was achieved at the 514-nm wavelength but not for the 488-nm beams. Losses on the order of 50% through the 50-m-long fiber were considered good because of the very small core diameter and relatively long length of these fibers. The system was operated at relatively low power because of the risk of damage to the expensive single-mode fibers. Care was taken to ensure that the linearly polarized beams were launched orthogonal to the fast axis of the birefringent fiber. The beams retain 95% linear polarization at the probe volume.

The linear bearings that permitted primary mirror translation were designed to kinematically limit motion to a single degree of freedom. Three pillow blocks were used, and bearing clearances were adjusted to be as tight as possible to eliminate probe volume deflection arising from hysteresis in the bearings. Orthogonal flexure mounts for the primary, secondary, and diagonal mirrors permitted independent differential thread adjustment for the alignment of each optic.

As with all confocal zoom designs, back reflections and scattering from optical components in the beam reaching the photomultiplier tube were a major concern. Antireflective coatings limited these reflections to a small fraction of the laser beam power, but even a minor specular reflection could overpower the very low intensity scattered light from the probe volume. A single on-axis mask was located on the collection lens (see Fig. 3) and effectively blocked unwanted scatter and reflections from the optics for the zoom ranges tested.

The spatial filtering efficiency of the light collection system was also evaluated. A scattering target was placed in the probe volume and the light intensity at the photodetector was measured. The scattering target was then moved along the optical axis and the reduction in intensity (resulting from the blocking of light by the spatial filter pinhole) was measured. It was found that at a distance of 10 mm in either direction along the optical axis from the beam intersection, the light level at the photodetector had dropped by 95%. This compares favorably with the ray trace predictions described earlier.

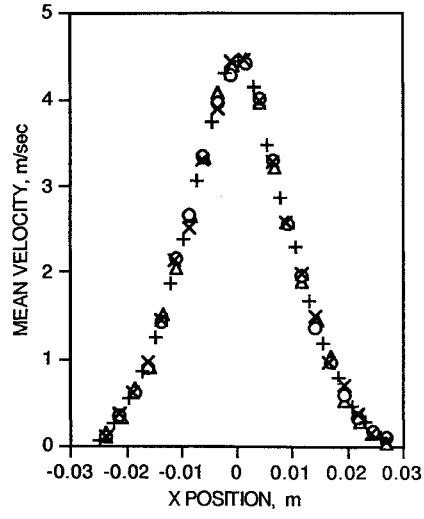

Fig. 5 Mean velocity profiles of jet axial velocity: +, blue; ×, green 1; o, green 2; and △, green 3.

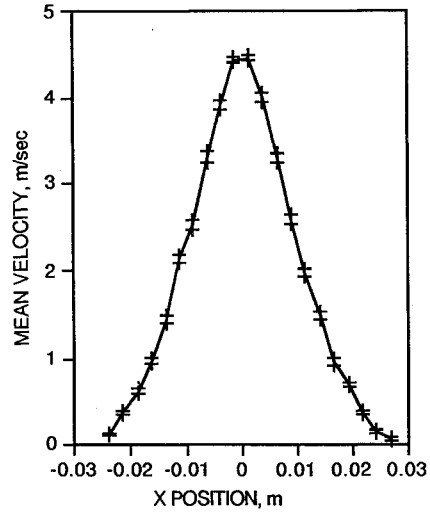

Fig. 6 Mean velocity and error limits for 95% confidence interval: ——, mean and +, error limits for 95% confidence.

Measurements on a low-speed air jet were made to evaluate the measurement capability of the system at near and far range. An air jet 0.0189 m in diameter seeded with mineral oil particles was discharged into room air. Axial velocity profiles were measured a distance of 0.075 m from the exit plane. Figures 5–7 present the axial velocity profile data obtained at a range of 3.08 m. The jet was oriented vertically for measurements with the 488-nm channel and then horizontally for measurement with the 514-nm channel. Three profiles were measured with the 514-nm channel to better evaluate repeatability.

These data show good agreement between the two (488- and 514-nm) optical systems and show good measurement repeatability. The mean velocity profiles show the expected triangular profile shape associated with the convergent shear layers in a turbulent jet. Error bars are plotted in Fig. 6 to provide an indication of the level of confidence in these mean value velocity measurements. Of course, one of the advantages of the ensemble-averaging procedure common with LV measurements is that the confidence interval may be narrowed significantly by simply taking large samples. Between 700 and 900 samples were typically acquired for each point in these profiles, except at the edges of the jet where seeding was sparse. The axial flow turbulence profile of Fig. 7 shows the expected peak in turbulence in the mixing annulus, with a somewhat lower value in the core where the mixing layers have not yet fully converged. Data rates were generally acceptable for these measurements in the range of 100–200 samples per second.

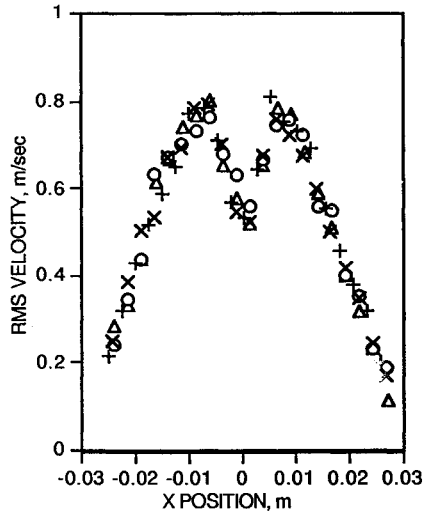

Fig. 7 RMS velocity profiles of jet axial velocity: +, blue; ×, green 1; o, green 2; and △, green 3.

These measurements also demonstrated the digital Fourier transform processor compatibility with the optical design of this system. Concerns related to the small probe volume diameter and corresponding short transit time were somewhat alleviated. However, testing at high speed may precipitate additional burst-duration-related problems.

Summary

A two-component dual-beam laser velocimeter system was designed and fabricated for use in the 40 × 80 ft wind tunnel at NASA Ames Research Center. The instrument design was based on the use of high-quality, large-aperture Schmidt–Cassegrain telescope optics to perform both the laser beam focusing and scattered light collection functions. The design relied on small probe volume size, which increased the laser power level in the probe volume and enhanced the spatial filtering mechanism for rejecting optical noise. Uncoupled orthogonal measurement of the streamwise and cross-stream velocity components could be made.

The optical components of the instrument were contained in a streamlined optical assembly that could be translated in the streamwise and cross-stream directions by means of a linear traverse assembly mounted to the wind-tunnel floor. The laser velocimeter probe volume was zoom translated in the vertical direction by focusing the primary mirror. On-axis backscattered light was collected through the same optical system and analyzed for Doppler shift. Single-mode polarization-maintaining fiberoptics transmitted light from the remotely located laser into the optical assembly. A multimode fiber conveyed the scattered light to remotely located photodetectors.

Because of the zoom feature of the system, many of the optical parameters related to system operation were range dependent. In particular, the magnification, fringe spacing, and probe volume diameter all varied linearly with range. Because optical sensitivity (fringe spacing) was range dependent, a range calibration of the instrument was required. Because the probe volume diameter increased with range, the probe volume intensity diminished at long range. However, since magnification is also increased with range, the size of the required spatial filter remained constant.

Frequency domain digital signal processing was selected for this application to enable the processing of Doppler signal with poor signal-to-noise ratio and a limited number of fringes. Several concurrent digital processing innovations were incorporated in the signal processor design. The processor permitted resolution of 0.4% of full scale and maximum velocity measurements to greater than the expected wind-tunnel speed.

The system was been fabricated, assembled, and evaluated in the optics laboratory. Good measurement repeatability and resolution were demonstrated. Adequate data rates were obtained.

References

[1]Yeh, Y., and Cummins, H. Z., "Localized Flow Measurements with an He-Ne Laser Spectrometer," *Applied Physics Letters*, Vol. 4, No. 10, 1964, pp. 176–178.

[2]Mayo, W. T., *Laser Doppler Flowmeters—A Spectral Analysis*, School of Engineering, Georgia Inst. of Technology, Atlanta, GA, 1969.

[3]Lourenco, L. M., "Particle Image Velocimetry: Photographic and Video Techniques," *Laser Velocimetry*, Vol. 2, von Kármán Inst. for Fluid Dynamics, Rhôde-Saint-Génèse, Belgium, 1991, pp. 1–30.

[4]Komine, H., Brosnan, S. J., Litton, A. B., and Stappaerts, E. A., "Real time, Doppler Global Velocimetry," AIAA Paper 91-0337, Jan. 1991.

[5]Reinath, M. S., "A Long-Range Laser Velocimeter," *Transactions on Aerospace and Electronic Systems*, Vol. 27, Inst. of Electrical and Electronics Engineers, New York, 1991, pp. 125–138.

[6]McGann, R. L., Caldwell, J. A., Hilton, S. M., and Soreide, D. C., "Three-Component LIDAR-Enhanced LDV Flow Diagnostics System," AIAA Paper 94-2646, June 1994.

[7]Dunagan, S. E., "Schmidt-Cassegrain Optics for Laser Doppler Velocimeter Applications," *Journal of Laser Applications*, Vol. 3, No. 1, 1991, pp. 27–35.

[8]O'Shea, D. C., *Elements of Modern Optical Design*, Wiley, New York, 1985, p. 217.

[9]Bachalo, W. D., and Houser, M. J., "Phase/Doppler Spray Analyzer for Simultaneous Measurements of Drop Size and Velocity Distributions," *Optical Engineering*, Vol. 23, 1984, pp. 583–590.

[10]Jensen, L., "Automatic Digital Signal Processing for LD," *Proceedings of the 4th International Conference on Laser Anemometry—Advances and Applications*, American Society of Mechanical Engineers, New York, 1991, pp. 617–628.

[11]Ibrahim, K. M., Wertheimer, G. D., and Bachalo, W. D., "Signal Processing Considerations for Low Signal to Noise Ratio Laser Doppler and Phase Doppler Signals," *Proceedings of the 4th International Conference on Laser Anemometry—Advances and Applications*, American Society of Mechanical Engineers, New York, 1991, pp. 685–692.